Solutions Spotlight

NEW! PlanCHECK™
Automated plan quality verification and reporting – available as part of the SunCHECK™ Platform

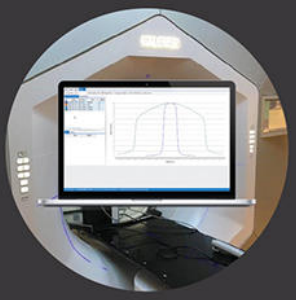

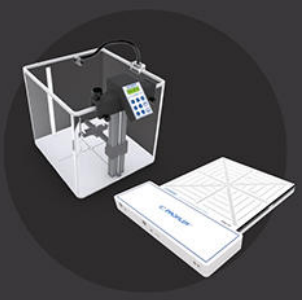

Varian Halcyon™ System Support
SNC Dosimetry™ v3.6 and 3D SCANNER™ for beam model verification and Halcyon Package for acceptance and verification

NEW! MultiPHAN™
An easy-to-use tool for comprehensive TG-142 daily alignment checks – verifying lasers to EPIDs to CBCT systems

Stereotactic Solutions
NEW SRS MapCHECK™ and StereoPHAN™ for end-to-end testing and Reference Detector for interference-free dosimetry scanning

MR-Based Radiotherapy
Custom patient and machine QA solutions, including ArcCHECK®-MR, IC PROFILER™-MR, MICRO+™ MR, and Solid Water® HE

See more. Learn more.
sunnuclear.com

SUN NUCLEAR corporation

Automated treatment planning for a dedicated multi-source intra-cranial radiosurgery treatment unit accounting for overlapping structures and dose homogeneity

Kimia Ghobadi[a] and Hamid R. Ghaffari[b]
Department of Mechanical and Industrial Engineering, University of Toronto, Ontario M5S 3G8, Canada

Dionne M. Aleman
Department of Mechanical and Industrial Engineering, University of Toronto, Ontario M5S 3G8, Canada; Institute of Health Policy, Management and Evaluation, University of Toronto, Ontario M5T 3M6, Canada; and Techna Institute, University Health Network, Ontario M5G 1P5, Canada

David A. Jaffray
Radiation Medicine Program, Princess Margaret Hospital, University Health Network, Ontario M5T 2M9, Canada; Department of Radiation Oncology, University of Toronto, Ontario M5S 3E2, Canada; Department of Medical Biophysics, University of Toronto, Ontario M5G 2M9, Canada; Institute of Biomaterial and Biomedical Engineering, University of Toronto, Ontario M5S 2J7, Canada; Techna Institute, University Health Network, Ontario M5G 1P5, Canada; and Ontario Cancer Institute, Ontario M5G 0A3, Canada

Mark Ruschin
Department of Medical Physics, Odette Cancer Centre, Toronto, Ontario M4N 3M5, Canada and Department of Radiation Oncology, University of Toronto, Toronto, Ontario M5S 3E2, Canada

(Received 13 March 2013; revised 6 July 2013; accepted for publication 22 July 2013; published 27 August 2013)

Purpose: The purpose of this work is to advance the two-step approach for Gamma Knife® Perfexion™ (PFX) optimization to account for dose homogeneity and overlap between the planning target volume (PTV) and organs-at-risk (OARs).
Methods: In the first step, a geometry-based algorithm is used to quickly select isocentre locations while explicitly accounting for PTV-OARs overlaps. In this approach, the PTV is divided into sub-volumes based on the PTV-OARs overlaps and the distance of voxels to the overlaps. Only a few isocentres are selected in the overlap volume, and a higher number of isocentres are carefully selected among voxels that are immediately close to the overlap volume. In the second step, a convex optimization is solved to find the optimal combination of collimator sizes and their radiation duration for each isocentre location.
Results: This two-step approach is tested on seven clinical cases (comprising 11 targets) for which the authors assess coverage, OARs dose, and homogeneity index and relate these parameters to the overlap fraction for each case. In terms of coverage, the mean V_{99} for the gross target volume (GTV) was 99.8% while the V_{95} for the PTV averaged at 94.6%, thus satisfying the clinical objectives of 99% for GTV and 95% for PTV, respectively. The mean relative dose to the brainstem was 87.7% of the prescription dose (with maximum 108%), while on average, 11.3% of the PTV overlapped with the brainstem. The mean beam-on time per fraction per dose was 8.6 min with calibration dose rate of 3.5 Gy/min, and the computational time averaged at 205 min. Compared with previous work involving single-fraction radiosurgery, the resulting plans were more homogeneous with average homogeneity index of 1.18 compared to 1.47.
Conclusions: PFX treatment plans with homogeneous dose distribution can be achieved by inverse planning using geometric isocentre selection and mathematical modeling and optimization techniques. The quality of the obtained treatment plans are clinically satisfactory while the homogeneity index is improved compared to conventional PFX plans. [http://dx.doi.org/10.1118/1.4817555]

Key words: Gamma Knife® Perfexion™, radiosurgery, fractionated radiotherapy, optimization, inverse planning, grassfire algorithm, sphere-packing, heuristic methods

1. INTRODUCTION

Stereotactic radiosurgery (SRS) is used in the treatment of various benign and malignant intracranial tumours, as well as neurological disorders. The Leksell Gamma Knife® (LGK) Perfexion™ (PFX, Elekta, Stockholm, Sweden) is capable of achieving the highly-conformal dose-distributions and steep dose gradients necessary for radiosurgery. Treatments with LGK technology typically involve a single-fraction of high-dose radiation with the use of a rigid head frame to accurately localize the target and immobilize the patient. In single-fraction radiosurgery (SF-RS), healthy brain tissue is

often spared by prescribing the radiation dose needed for cure where the dose fall-off is rapidly occurring (e.g., the 50% isodose line), thereby accepting a higher and heterogeneous dose within the target itself.

The use of SF-RS has been demonstrated to be safe and effective for treating small target volumes. The limiting factor for treating larger volumes is the risk of radiation-induced necrosis. There is evidence to indicate that the risk of radiation-induced necrosis increases substantially if the volume of normal brain receiving 12 Gy in a single fraction exceeds 10 cc.[1] Therefore, for such cases where larger target volumes are concerned, it may be beneficial to divide the radiation dose into several fractions to provide extra sparing to the healthy tissue while still maintaining a high dose per fraction. For fractionated treatments, Elekta commercially released a relocatable head-frame that has been demonstrated to provide accurate daily setup and immobilization when used in conjunction with image guidance.[2,3] Although not the convention for LGK radiosurgery, there is motivation for the incorporation of a strategy to account for the small, yet finite, daily setup variation present with relocatable head frames to ensure complete tumour coverage by the prescription dose.[2] One such strategy could involve planning each individual fraction, but this strategy would require additional CT scans and resources, and does not address any systematic error in setup between the CT couch and the treatment couch. A simpler strategy would be to adopt the ICRU guidelines [ICRU Report Nos. 50, 62, and 83 (Refs. 4–6)] to use a planning target volume (PTV), to account for setup uncertainty. The present study addresses the situation in which a PTV may be applied to account for setup uncertainty.

The application of a PTV in LGK radiosurgery is a nontrivial task, since the dose gradients involved are conventionally very steep. If the dose is prescribed to the periphery of the PTV, then the visible tumour would receive a substantially larger mean dose. Furthermore, the PTV may overlap with critical organs such as the brainstem, which poses a challenge in terms of sparing those organs. When an overlap between the PTV and the surrounding organs-at-risk (OARs) exists, any inhomogeneity in dose distributions may result in hotspots in the overlap region and subsequently overdose in the OARs. Therefore, the aim of the present work is to develop a process by which more homogeneous dose distributions can be automatically generated, thus giving clinicians the option to incorporate PTVs in their practice. In our proposed approach, the prescribed dose would cover the boundary of the PTV and there would be only a minimal increase in dose towards the centre of the tumour. In such cases where the prescription dose would exceed normal tissue tolerances, the algorithm should be made flexible to allow for clinician-driven decisions as to whether to compromise coverage in the overlap region (PTV with the critical organ) and by how much.

The ability of PFX to easily deliver complicated treatments combined with recent advances in mathematical optimization models to obtain inverse treatment plans[7] may allow PFX to be used to deliver homogeneous treatment plans. In PFX, the radiation is emitted from eight collimator banks (called sectors) that are positioned around the patient's head. Each sector can deliver radiation beams independently from other sectors by opening one of its three collimators (with sizes 4, 8, and 16 mm) or blocking all the collimators. The simultaneous beams radiated from various sectors all focus at one point which is called an "isocentre."

There has been limited previous research in LGK radiosurgery treatment optimization[7–13] due to the impracticality of delivering complex treatments clinically with older LGK models. One previous study[7] involved developing automated SF-RS treatment plans for LGK PFX, focusing primarily on the concepts of conformality and steep dose gradients. Manual forward planning for multifraction radiosurgery (MF-RS) is more challenging than SF-RS because more isocentres are generally needed to achieve more homogeneous dose plans.

The purpose of this study is to develop and test an algorithm capable of automatically generating treatment plans with homogeneous dose distributions that can handle overlapping structures without violating the OAR dose constraints. The isocentre locations are obtained using a fast algorithm based on geometry of target volumes and presence of OARs in the treatment area. For the obtained set of isocentres, a mathematical optimization model is employed to determine the optimal duration of each collimator size at each sector, similar to the approach used in the previous examination of PFX inverse planning,[7] but with improved geometric considerations and explicit handling of OARs.

2. METHODS AND MATERIALS

In designing an inverse plan for PFX, we first select the spatial locations of the isocentres (Sec. 2.A). Next, we feed those isocentre locations into a convex quadratic optimization model, called the sector duration optimization (SDO) problem, presented in a previous study,[7] to determine the optimal sizes and durations of the collimators in each sector at every isocentre location (Sec. 2.B).

2.A. Isocentre selection

An isocentre is the focal point of the beams of radiation, and therefore, any point within the PTV is a candidate isocentre location. For simplicity, we treat PTV voxels as candidate isocentre locations. Isocentres must be chosen in such a way that appropriate radiation can be delivered to the targets while avoiding excessive dose to OARs. In MF-RS, it is common for overlaps to exist between the PTV and OARs, and for those overlaps to contain a significant number of voxels. To visually demonstrate the volume and severity of overlaps, we use overlap volume histograms (OVHs).[14] An OVH shows a histogram of a structure's normalized volume and distance to a target volume. Figure 1 shows a representative OVH (Case 6), and Table III shows the percentage overlap between the PTV and nearby OARs for all test cases, as well as other case details.

Due to the significant overlap with the healthy structures created by the PTV in MF-RS plans, special consideration of PTV-OAR overlaps is necessary in isocentre location selection for MF-RS. However, the only previous isocentre

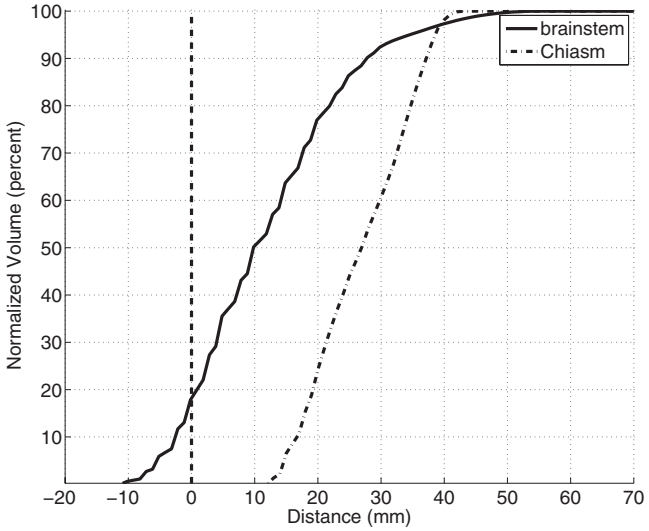

FIG. 1. Overlap volume histogram (OVH) between the PTV and OARs in a representative case (Case 6). The dotted line at zero indicates where the PTV is located. In this case, about 20% of the brainstem is inside the PTV, with a maximum overlap depth of 13 mm. The chiasm has no overlap with the PTV.

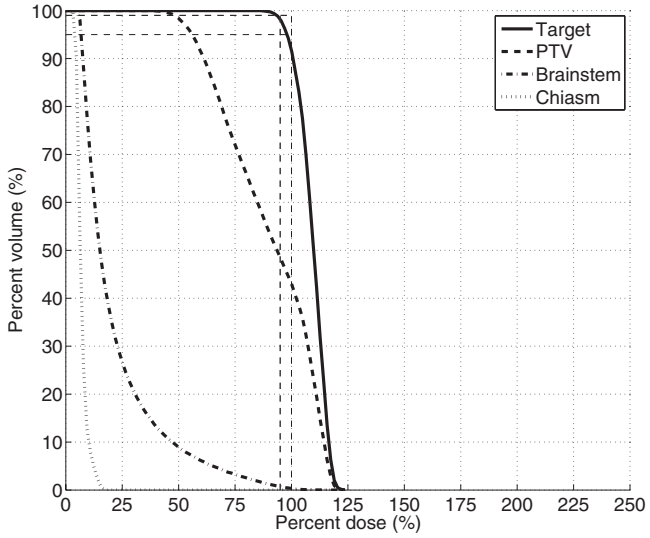

FIG. 2. The dose volume histogram of the target and nearby OAR structures for a representative case (Case 1) of an MF-RS plan with 55 isocentres selected using a GSP method previously presented in the literature,[7] but with optimization weights tuned for MF-RS. The obtained plan is homogeneous, but at the cost of severe underdose to both the GTV and PTV.

selection method presented for PFX—a combined grassfire and sphere-packing (GSP) approach[7]—focused on SF-RS, where overlaps between the target and OARs were not present, and therefore the dose distribution was not required to be homogeneous. Table I illustrates the plan quality for the test cases that were presented in their study.[7] As the table shows, the homogeneity index, which is defined as the ratio of the maximum delivered dose to the prescription dose, is on average 1.47, which may result in hotspots in the OARs in MF-RS plans. To obtain homogeneous MF-RS plans, we first used the same isocentre selection method and optimization model in a previous study,[7] but with a larger number of isocentres in the PTV to improve homogeneity. We tuned the weights in the optimization model specifically to try to achieve acceptable GTV, PTV, and brainstem dose for an MF-RS plan. Figure 2 shows the dose-volume histogram for a representative case (Case 1) when 55 isocentres are selected in the PTV. Although the obtained MF-RS plan is homogeneous, both the GTV and PTV are severely underdosed (with GTV $V_{99} = 93.5\%$ and PTV $V_{95} = 48.5\%$, while the clinical guideline requires $V_{99} \geq 99\%$ and $V_{95} \geq 95\%$, respectively), and the 1 mm^3 brainstem is overdosed by 1.2 Gy.

TABLE I. Plan quality summary for SF-RS plans tested on seven clinical cases using the GSP approach previously presented in the literature.[7]

Case	Isocentres[a]	GTV - V_{99}	HI[b]	Brainstem dose[c] (Rx%)	Solution time (min)
1	25	99.0	1.53	109	74
2a	40	99.5	1.56	21	107
2b	45	99.5	1.44		
3	35	99.2	1.29	102	53
4a	3	99.3	1.28		
4b	40	99.5	1.44	11	762
4c	20	99.1	1.37		
5	20	99.4	1.50	110	350
6	50	97.7	1.70	124	33
7a	10	98.6	1.54	113	129
7b	35	98.4	1.55		

[a]Number of isocentres in inverse plans obtained by GSP algorithm.
[b]Homogeneity index.
[c]Maximum dose to 1 mm^3 of brainstem relative to the prescription dose.

To obtain isocentres for clinically acceptable MF-RS plans, we propose three extensions to the GSP method that explicitly incorporate the PTV-OAR overlaps in MF-RS: (1) improved scoring of isocentre locations; (2) the ability to place isocentres from outside in, rather than the inside out (which we call shallow placing); and (3) the ability to prefer isocentres near the boundary (which we call cropping). This section provides a conceptual description of each of these extensions, followed by a description of the complete modified GSP procedure. Algorithmic steps are given in the Appendix.

2.A.1. Grassfire and sphere-packing overview

The basic concept of GSP is to find the deepest voxels in a given volume, and then select the "best" of those deepest voxels to be an isocentre location.[7] A grassfire algorithm[15] is used to determine the deepest voxels in the target volume and their actual depths, while a scoring technique based on several metrics is performed to determine the best isocentre, which is then used in the treatment. The sphere-packing component is that we place the largest "sphere" of radiation that PFX can deliver (a sphere of diameter 4, 8, or 16 mm depending on the maximum depth of the target volume) at that best isocentre, and then say that those voxels covered by the sphere are removed from the target volume. Next, grassfire is again used to find the deepest voxels, and the process continues until the depth of the remaining target voxels is sufficiently small (i.e., sufficient coverage is achieved).

The "sphere" of radiation assumed by GSP is actually not a sphere, but a spherical cloud which we define as follows. Say the largest sphere that can fit at the chosen isocentre has radius r. A spherical cloud is any shape, sphere or otherwise, that fits between a sphere of radius $r(1-f)$ and a sphere of $r(1+f)$, where both spheres are centred at the chosen isocentre and $f<1$ is a parameter of the GSP algorithm. For simplicity, we will refer to a spherical cloud at a particular isocentre location as a "shot" in the remainder of this section. It is important to note that the spherical cloud assumption is only used to facilitate isocentre selection based on structure geometry, and that actual radiation delivery shapes are determined solely in the SDO phase (Sec. 2.B). Any collimator sizes obtained during isocentre selection will be disregarded in the SDO phase. The final treatment plans have no requirement to contain spherical or spherical cloud shapes.

For more details of the original GSP method, we refer the reader to the original publication.[7]

2.A.2. Improved scoring

The scoring method to select the "best" isocentre is described in detail in Sec. 2.A. of the original GSP study.[7] The scores are evaluated based on (1) the proximity of the voxels to the boundary, (2) the volume of the overlap that the new shot will create with previously chosen shots, and (3) the dose spillage outside the target. We improve upon the scoring technique in our method by improving the calculation of the proximity of the voxels to the target boundary. Previously, a voxel's distance to the boundary was calculated using a bounding box approximation.[7] Instead of this approximation, we now use an actual calculation of the distance to the boundary.

We use the voxel-to-boundary distances to determine whether the target is irregularly shaped, which requires a higher density of isocentre locations to achieve satisfactory radiation delivery. If the distance is short in one dimension and long in another, then we conclude that the target is irregularly shaped in that area, and so we give higher scores to the voxels in the irregular area so that they are more likely be selected as isocentre locations.

We also employ different methods of isocentre selection based on the distance of the target voxel from the surrounding OARs. As Fig. 4 illustrates, we divide the PTV into PTV-OAR overlap volume ($\mathcal{OT}$), the volume immediately adjacent to the overlap ($\text{Ring}_{\mathcal{OT}}$), and then the rest of the PTV. Sections 2.A.3–2.A.4 explain the isocentre selection methods, and Sec. 2.A.5 provides more details on the division of the PTV to sub-volumes.

2.A.3. Shallow placing option

When selecting the isocentres, the location of the new isocentre is chosen with respect to the size and location of the previously chosen isocentres. The scoring method in GSP accounts for this relation between the location of the isocentres by encouraging voxels located further from previous isocentres as the new isocentre location, and also by avoiding large overlaps with previous shots (based on the value of the parameter f). Therefore, at each iteration, the isocentres that are already chosen impose a restriction on the feasible set of voxels which can be used for the new isocentre. Placing the isocentre in the middle of the target, as done in the original GSP, creates a large restriction because it can break the target volume into smaller sub-volumes which can only be covered with small shots. However, if we place each isocentre as close to the boundary as possible, so that the boundary of the shot follows the boundary of the target properly, then we impose less restriction on the location and size of the next isocentres. This location flexibility occurs because shots that are placed close to the boundary affect a smaller area of the target as opposed to the shots that are placed in the middle of the target. We refer to this approach, where the shots are placed close to the boundary, as shallow placing option.

In the shallow placing option, we start placing isocentres that are located near the surface of the target and then proceed to place isocentres more deeply. First, a grassfire algorithm is performed to obtain the depth of each voxel in the structure. We use the maximum depth of the structure to identify the largest collimator size. Once the largest collimator size (and therefore the radius of the spherical shots) is found, we find those voxels that have the same depth as the largest radius, and select the best of those voxels as the next isocentre location. We then remove all the voxels that are inside the new shot and repeat the process until the depths of voxels in the structure are sufficiently small.

By starting to place the isocentres from the boundary, the shots can be better aligned with the boundary compared to placing the shots from inside out, so shallow placing can be particularly beneficial for irregularly shaped targets. The shallow placing option also helps to maintain the connectivity of the remaining target volume after placing each shot. In the original GSP, after placing the shots at centre, the target volume may break into smaller volumes. These smaller volumes may each require many small shots to be covered, while if connected, fewer large shots may provide the same coverage.

2.A.4. Cropping option

In the cropping option, only a few isocentres with large collimator radii are selected in the central volume of the structure (cropping out the middle of the target), and the focus is shifted to carefully positioning the rest of the isocentres along the boundary of the target. For this purpose, the target volume is separated into two distinct volumes which are assigned isocentres sequentially: (1) a cropped volume ($\mathcal{CV}$), where the few large shots will be placed; and (2) a boundary ring ($\mathcal{BR}$), where the isocentre placement will be focused. These structures are illustrated in Fig. 4.

The boundary ring includes all voxels that are closer than distance r_t to the boundary, and the cropped volume contains the remaining voxels. The parameter r_t can be user-specified or calculated automatically. In our test cases, we find that choosing 4–6 mm distance for r_t experimentally results in good isocentre selection because the smallest collimator size

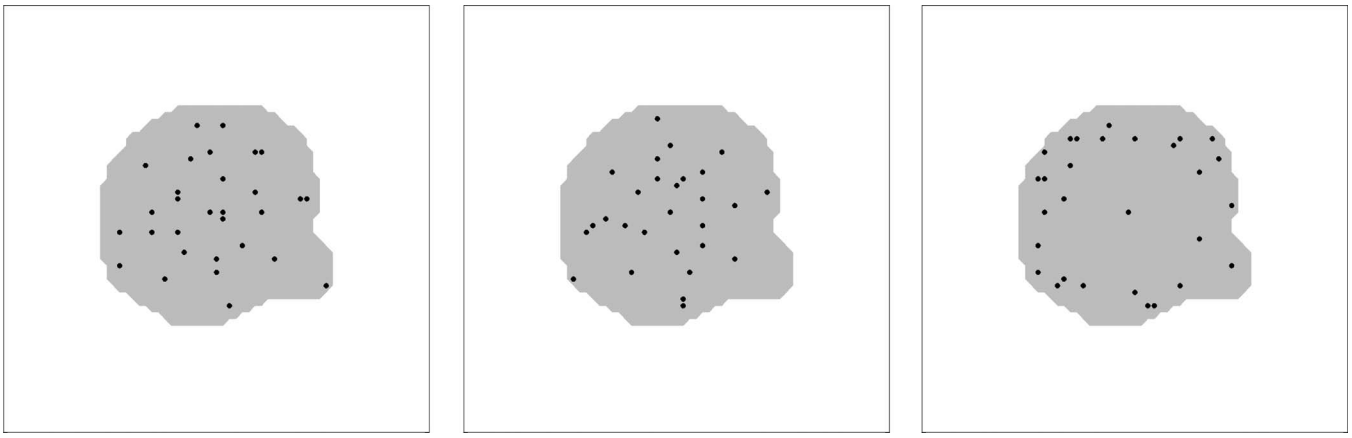

FIG. 3. Isocentre selection options for a representative case (Case 1) with 30 isocentres. (Left) regular GSP with improved scoring. (Centre) shallow placing option. (Right) cropping option with a 4 mm boundary ring.

is 4 mm, and therefore the boundary ring can be covered with the smallest collimator size.

The number of isocentres required to provide a coverage for the cropped volume can either be a user input, or calculated based on the volume of the cropped section while assuming the largest collimators possible as the radius of the spheres. The cropping option is beneficial to find isocentre locations in large targets (10 cm^3 or larger based on our experiments).

2.A.5. Modified grassfire and sphere-packing procedure

Figure 3 illustrates the isocentres selection with the different GSP placement options. In the shallow placing option, the isocentres are more scattered throughout the target. Therefore, to achieve the same boundary coverage in large target volumes, a higher number of isocentres may be required compared to the cropping option. However, in small or irregularly shaped targets, shallow placing is more flexible in capturing the irregularities than cropping, and the cropping option will result in a small boundary ring and/or cropped volume that may require a higher number of isocentres, be too small to contain any isocentre, or lead to dose spillage outside the target. Thus, it is beneficial to apply different isocentre selection options in different regions of the target. The flexibility to impose different isocentre placement options is especially important to properly handle PTV-OAR overlaps, where it may be beneficial to place many isocentres near the boundary of the overlap in such a way that the PTV-OAR overlap is tightly contoured, but the spillage into the PTV-OAR overlap is sufficient to achieve proper PTV coverage.

In order to perform different isocentre selection methods on different parts of the target, we create several artificial structures inside the target and perform different GSP variations in each. The set of isocentres obtained from each of the new structures provides the final isocentre locations for the treatment. Figure 4 (left) illustrates the artificial structures created for a PTV ($\mathcal{T}$) with a single overlapping OAR ($\mathcal{O}$). We label the region of overlap $\mathcal{OT}$, and then extend $\mathcal{OT}$ by a radius of r_o into the target; the voxels in this extended area are called $\text{Ring}_{\mathcal{OT}}$. Empirically, r_o is chosen to be 4–5 mm so that $\text{Ring}_{\mathcal{OT}}$ can be covered with shots of 4 mm radius, the smallest collimator size. These artificial regions are created

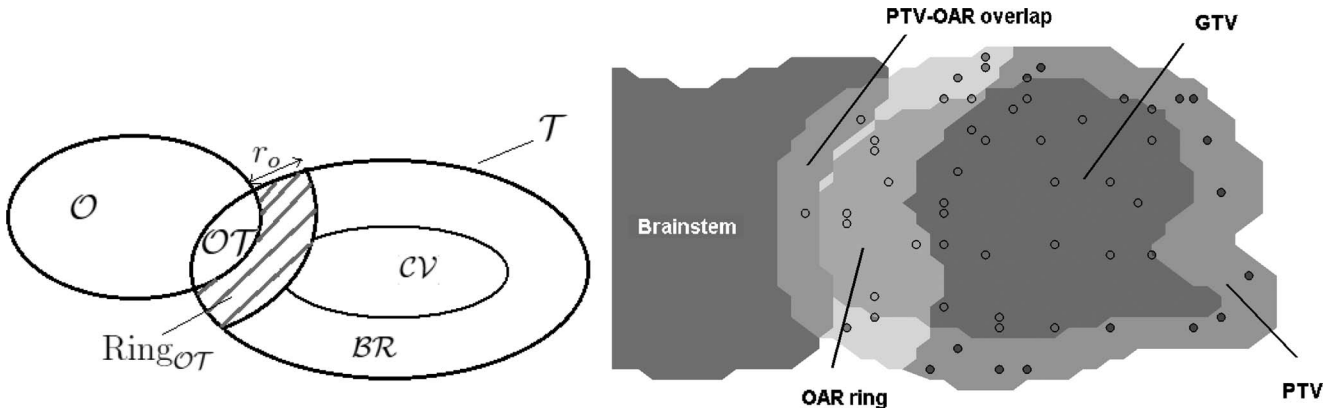

FIG. 4. Illustrations of artificial regions for isocentre selection. (Left) The overlap area ($\mathcal{OT}$) between the target ($\mathcal{T}$) and the OAR ($\mathcal{O}$) is separated from the rest of the target along with a voxels close to the overlap volume ($\text{Ring}_{\mathcal{OT}}$ with radius r_o); structures $\mathcal{BR}$ and $\mathcal{CV}$ are used in the cropping option only. (Right) Isocentre selection on a representative clinical case with 55 total isocentres (two isocentres in the PTV-OAR overlap, 18 in the OAR ring, and 35 in the pure PTV).

TABLE II. Isocentre selection options for the various artificial target structures.

Structure	Isocentre placement option
Pure target ($\mathcal{T}'$) <10 cm^3	Regular GSP
Pure target ($\mathcal{T}'$) ≥ 10 cm^3	GSP with cropping option
Cropped volume ($\mathcal{CV}$)	Regular GSP
Boundary region ($\mathcal{BR}$)	GSP with shallow placing option
PTV-OAR overlap ($\mathcal{OT}$)	Regular GSP
Overlap ring (Ring$_{\mathcal{OT}}$)	GSP with shallow placing option

for every OAR that overlaps with the PTV. After identifying artificial structures, the remainder of the pure target is called $\mathcal{T}'$.

Table II shows the isocentre placement options used in each artificial structure. Figure 4 (right) illustrates the final isocentre locations for a representative case (Case 1), where the brainstem overlaps with the PTV.

2.B. Sector duration optimization algorithm

Once the locations of all the isocentres are found, the locations (and not their collimator sizes) are input into the sector duration optimization model, which optimizes the duration of the collimator sizes at all isocentre locations, simultaneously. The SDO model is a penalty-based model in which the deviation of the delivered dose from the prescription dose for every structure is minimized. The decision variables in this model are the radiation time for every collimator size in each sector (therefore a total of $8 \times 3 = 24$ variables) for every isocentre location. This convex problem only has a non-negativity constraint as the irradiation time cannot be negative, and it is solved using a projected gradient algorithm.

This model, which is similar to the fluence map optimization (FMO) model in intensity modulated radiation therapy (IMRT) literature, is previously presented for SF-RS plans.[7] In this work, we employ the same optimization model but additionally incorporate the artificial structures shown in Fig. 4 and use two different sets of weighting parameters in the objective function to accommodate the larger and more complex cases and homogeneity requirements in MF-RS compared to SF-RS plans. One parameter set is for cases in which there is no OAR overlap with the target, and therefore better conformity of PTV and GTV can be achieved. Another set of parameters is used when the OARs overlap with the target volume. In this set of parameters, more emphasis is placed on sparing the OARs compared to achieving PTV coverage.

In this approach, we compute 24 dose-rate distribution kernels, where each distribution kernel corresponds to a sectors-collimator combination (8 sectors $\times$ 3 collimator sizes). Since the input for the SDO model is the number and location of isocentres, the radiation delivery time for each sector-collimator combination is optimized in the SDO model. The dose at each iteration is computed as a linear sum of the initial dose-rate kernels multiplied by the corresponding beam-on time. After the SDO model finishes, the radiation delivery times for each sector-collimator combination for a given isocentre are analyzed to form deliverable shots that may consist of different collimator sizes for each sector being used simultaneously.

2.C. Evaluation of the algorithm

The algorithm was implemented in Matlab 2008b (The Mathworks, Inc.) on a Quad-Core AMD Opteron™ Processor 2354 MHz in Redhat-CentOS-5.5 platform with 40 GB RAM. In terms of computation, each additional isocentre adds 24 variables to the problem, and therefore the problem size increases linearly. The computational requirement is highly dependent on the number of voxels, and therefore varies significantly from case to case. This approach was tested on seven clinical cases comprising 11 targets that were treated with different modalities and fraction regimens as indicated in Table III.

TABLE III. Specifications of the tested clinical cases.

	Clinical			GTV		PTV		PTV overlap %			
Case	Indication	tx method	Rx (Gy)	Volume (cm^3)	Number of voxels	Volume (cm^3)	Number of voxels	BS	Cl	CnV	Total number of voxels
1	AN	linac-RT	50	8.56	7 178	18.51	15 535	10.2	…	…	56 856
2a	MM	PFX-MFRS	24	17.72	34 763	25.87	50 756	0	…	…	187 593
2b			in 3	11.71	22 973	17.57	34 467				
3	AN	PFX-SFRS	12	1.28	3 788	2.16	6 394	4.9	0	…	31 740
4a	MM	PFX-MFRS	24	0.85	2 058	1.80	4 345	0	…	…	203 541
4b			in 3	25.81	62 241	34.36	82 849				
4c				5.66	13 637	8.75	21 108				
5	AN	linac-RT	50	5.08	5 037	12.33	12 226	12.8	0.1	1.1	74 528
6	AN	linac-RT	50	13.06	13 159	56.49	23 693	10.9	…	…	53 751
7a	MM	PFX-SFRS	15	0.19	328	0.50	860	37.7	…	…	45 493
7b				2.71	4 617	4.37	7 64	23.0			
Mean	…	…	…	8.42	15 434	16.61	23 609	12.4	0.1	1.1	66 874
St. dev.	…	…	…	8.05	18 617	17.06	24 505	12.7	0.1	0	49 219

AN = acoustic neuroma. MM = multiple metastases. BS = brainstem. Cl = Cochlea. CnV = Cranial nerve V.

TABLE IV. Plan quality summary for radiotherapy with prescription doses of 50 Gy to both the GTV and PTV.

Case	Isocentre[a]	GTV - V_{99}		PTV - V_{95}		HI[b]		Brainstem[c] (Rx%)		Solution time (min)
		Clin	Inv	Clin	Inv	Clin	Inv	Clin	Inv	
1	55	100.0	99.7	99.3	93.9	1.07	1.20	103.4	106.8	111
2a	40	99.9	100.0	95.1	98.2	1.75	1.15	42.5	45.8	304
2b	25	99.9	99.8	95.3	96.6	1.75	1.18			
3	50	98.4	99.6	...	97.2	2.22	1.16	128.5	102.6	110
4a	5	100.0	100.0	95.3	96.9	1.34	1.10			
4b	50	99.9	99.1	94.8	94.3	1.69	1.27	26.2	35.4	359
4c	20	100.0	99.9	96.5	93.0	1.54	1.18			
5	53	99.6	99.8	98.9	94.4	1.05	1.24	101.2	107.4	128
6	104	100.0	100.0	99.3	93.4	1.08	1.23	104.6	107.8	183
7a	30	98.5	100.0	...	91.7	2.06	1.12	112.6	107.8	239
7b	51	97.3	99.3	...	90.6	1.97	1.18			

Clin: clinical plans. Inv: inverse plans.
[a]Number of isocentres in inverse plans obtained by GSP algorithm.
[b]Homogeneity index.
[c]Maximum dose to 1 mm^3 of brainstem relative to the prescription dose.

As presented in Table III, the cases considered in the this study vary in prescription dose, fractionation, and treatment approach. Furthermore, various PTV margins were used, and for Cases 3 and 7, no clinical PTV margin was provided at all. For Cases 3 and 7, we generated a 5 mm expansion of the GTV to form a PTV, whereas we used the clinically-derived PTV for all other cases.

For the present study, we applied a consistent planning approach to all cases as follows: (1) At least 99% of the GTV must receive greater or equal to the prescription dose, i.e., V_{99} (GTV) $\geq$ 99; (2) at least 95% of the PTV must receive greater or equal to 95% of the prescription dose; and (3) the maximum dose to 1 mm^3 of brainstem must not exceed 108% of the prescription dose for MF-RS or 15 Gy if SF-RS. For clinical realism, any shots with duration less than 10 s were removed from the treatment plan. The homogeneity of the obtained plans were measured using homogeneity index (HI).[16]

3. RESULTS

We tested our approach on the seven clinical cases, and the isocentre selection procedure for all the plans was performed in less than 20 s, and the computational time for SDO was on average 205 min (Table IV). The SDO computational time includes no parallelization of the algorithm. In the present results, we found that it is more difficult to simultaneously spare the brainstem and achieve $V_{95} = 95\%$ for PTV in cases with high PTV-brainstem overlap such as Cases 1, 5, 6, and 7.

In Table IV, we present the results from our inverse planning approach (Inv) and the clinically delivered plans (Clin). Since the clinically delivered plans are diverse, we cannot apply an "apples-to-apples" comparison between our results and the clinical results. However, by comparing the standard plan quality metrics (including homogeneity index and dose to OARs), we can quantify the differences between the plans, even though some degree of differences are expected among various planning and delivery devices. For instance, inverse plans are far more homogeneous than the Perfexion-based plans (average 0.62 improvement), but slightly less homogeneous than the linac-based plans (average 0.16 worse).

The obtained GTV coverage for all 11 targets is clinically satisfactory as shown in Table IV. The PTV coverage was adequate in four of the targets, with a minimum PTV coverage of $V_{95} = 90.6\%$ (Case 7b). The case with the lowest PTV coverage had 23% of the PTV overlapping with the brainstem. Among the seven PTVs with low coverage, five of them had at least 10% overlap with the brainstem. The mean PTV coverage, over all the cases, was $V_{95} = 94.94\%$ with standard deviation of 0.02%. The HI in the inverse plans is slightly higher than linac-based plans (Cases 1, 5, and 6) but much lower than PFX-based plans, with an overall average of 1.18.

Table IV also illustrates that the brainstem dose met the clinical guidelines or was less than clinically delivered dose in all the targets. As expected, for the cases treat with linac-based external beam radiotherapy (Cases 1, 5, and 6), the brainstem doses on inverse-planned PFX was slightly higher than for the clinically derived distributions, but all were less than 108% of the prescribed dose. The right and left lenses were spared in all the plans with mean doses of 3.5 and 4.8 Gy in a 50 Gy prescription dose plan with standard deviations of 1.7 and 2.3 Gy, respectively.

The quality of the plans were also examined with the dose-volume histogram (DVH) and isodose lines figures. Figure 5 illustrates these measures for a representative case (Case 1) for a plan with 55 isocentres. The DVH figure indicates the degree of homogeneity achieved with HI ratio of 1.20.

4. DISCUSSION

The results of the present study indicate that it is possible to achieve more homogeneous dose distributions and account for PTV margins and OAR-target overlaps with inverse-planned PFX across a spectrum of diseases. Dose inhomogeneity is widely accepted in radiosurgery, particularly with the Gamma Knife®. Regions of dose up to 200% or more of the prescription ("hotspots"), that are well-contained

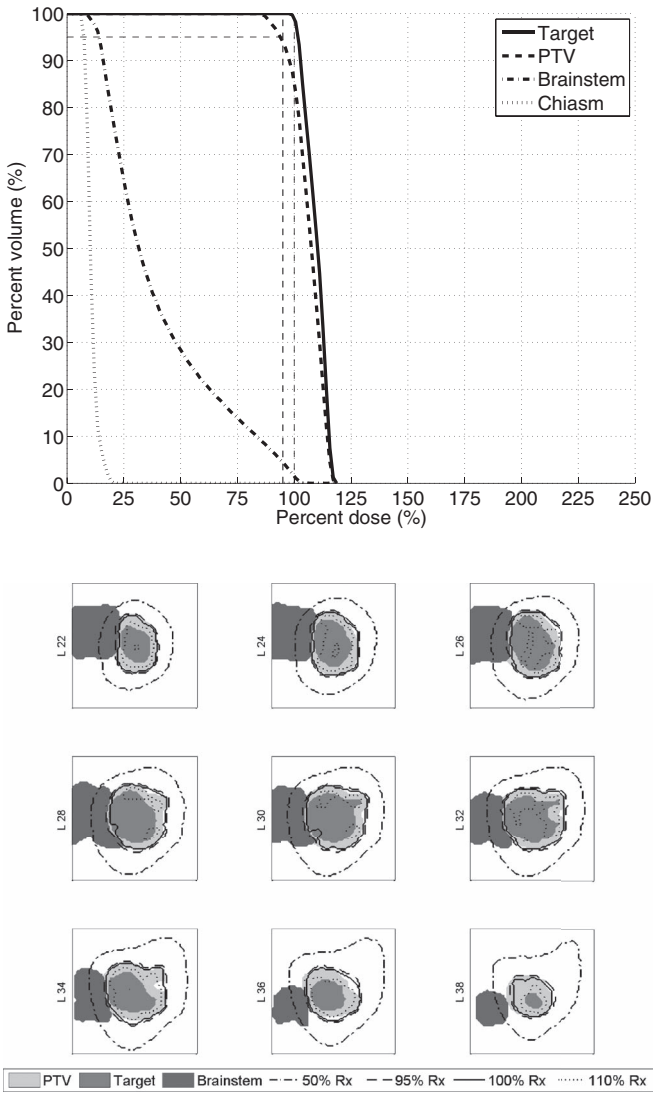

FIG. 5. Dose-volume histogram and isodose lines of the target and nearby OAR structures for a sample case (Case 1) using 55 isocentres with HI 1.20. 100% dose refers to 50 Gy in this case. (Top) Dose-volume histogram for the target (solid line) and OARs (dashed gray lines). The V_{100} is also indicated with vertical and horizontal dashed lines. (Bottom) Cross-sectional views of the target and brainstem showing the conformal prescription isodose line ("100% Rx") as well as 50%, 95%, and 110% of the prescription isodose.

within the diseased region, can exist in SF-RS plans. However, a study by Ruschin *et al.*[2] reports on uncertainty in patient setup using the relocatable frame designed for PFX. Even with cone-beam CT image guidance, there is residual uncertainty in setup that requires a strategy to ensure that the target receives the full prescription dose. Therefore in the present study, we use a PTV for handling these uncertainties as recommended by the ICRU guidelines (ICRU Report Nos. 50, 62, and 83[4–6]).

However, it is not straightforward to apply ICRU principles when prescribing dose to the surface of the PTV as is done for SRS. Firstly, it is impractical to manually generate heterogeneous plans that absolutely guarantee that no hotspots will arise in healthy tissue between the surface of the PTV and the surface of the delineated target (i.e., such as when the PTV overlaps an OAR). Using a homogeneous dose distribution ensures that the target is guaranteed the prescription dose, while adjacent or overlapping OARs are guaranteed to not exceed the prescription dose.

Secondly, reporting of dose from heterogeneous dose distributions is challenging since these distributions cannot readily be parameterized into one or two simple variables. The ICRU recommends a limit of dose variation within the PTV of $+7\%$ to -5% to facilitate reporting. In the context of clinical studies and patient outcomes, a patient series in which dose distributions were all heterogeneous is much more difficult to interpret than a patient series in which dose distributions were all uniform. For example, it is difficult to model tumour control probabilities resulting from complex three-dimensional heterogeneous dose distributions.

There are several papers that address uncertainty in daily setup variation although none make specific recommendations as to what to use as a PTV margin. The PTV margins used in our study were derived from clinical cases used at our institution with in-house data, as well as data published by Ruschin *et al.*[2] In their study, the relocatable head frame (Extend for Perfexion) was evaluated on 14 patients using CBCT image analysis. Based on those data, when using the Extend system for multisession treatments, a PTV margin of 1.5 mm–2 mm is used. The interfraction and intrafraction performance of the Extend system is also later analyzed using the "depth helmet" approach,[17] with similar results to Ruschin *et al.*, but no means of addressing rotations and a somewhat smaller uncertainty in sup-inf direction. Another paper investigates four frameless mask-based approaches and generally concludes that with daily image-guided pre-treatment corrections, a PTV margin of 1 mm would generally be acceptable.[18] The purpose of our work is not to focus on what exactly the PTV margin is or should be, but simply how to address it in the context of treatment planning optimization.

Prescribing and reporting dose using PTV introduces some limitations compared to SRS, including larger treated volume, difficult optimization, larger treatment times, however, using a PTV is in accordance with the ICRU standards that has had proven safe and effective in radiotherapy. The homogeneity in dose distribution in the PTV ensures that the target receives the prescription dose while the overlapping OARs are spared from receiving excessive dose.

The homogeneity level achieved by our approach, as expected, was lower for the cases that were originally planned for linacs using IMRT, since such a homogeneous PFX plan would require a prohibitively large number of isocentres. Nevertheless, we achieved an average HI of 1.22 in the PFX plans for the cases originally planned on a linac and only marginally higher (and clinically acceptable) brainstem doses. For the cases originally planned on PFX, the inverse plans were substantially more homogeneous, and the cases where the target bordered on the brainstem had lower brainstem dose due to the improved homogeneity.

The large amount of OAR and PTV overlap in the tested cases and the fact that our treatment plans commonly resulted in PTV underdose suggests that a fundamental trade-off

must be made between target coverage and organ sparing. The OVHs and the PTV overlap percentages support the need for a trade-off by illustrating the amount of overlap in the PTV and the brainstem in our cases. The largest PTV overlap is in Case 7 with 38% and 23% overlap, while some cases exhibited no overlap.

The main obstacle to employing this planning approach clinically is beam-on time. In this study, we did not consider the efficiency of the dose delivery in our optimization model. The average beam-on time per fraction per dose was 8.6 min. Since achieving more homogeneous dose distributions requires additional isocentres compared to traditional Gamma Knife® planning, the beam-on time is consequentially larger. In the case of MF-RS, the beam-on time per fraction will of course be somewhat shorter, but the overall the treatment time will be large. It should be noted that we did not consider beam-on time explicitly in the optimization model. Future work will include techniques to incorporate the beam-on time in the optimization model, for instance, the beam-on time can be added as a penalty term to the objective function of the SDO model.

Another potential limitation of the present study relates to isocentre selection method. In the presented approach for fractionated RS plans for LGK, unlike previous approaches,[7–12] our isocentre selection method is specifically designed to handle large GTV and PTV target volumes as well as emphasize dose homogeneity in the final treatment. However, our isocentre locations are not necessarily the optimal isocentre positions, and therefore the plans may not be optimal. From the results, it can be deduced that, even though sub-optimal, the plans are very good based on the clinical objectives. Including the isocentre location in the optimization model will result in mixed-integer optimization problems which are more complex and computationally expensive to solve. The two-step approach of isocentre location and SDO model presented here is not unique to LGK,[7] but is the common approach in IMRT literature, where gantry and collimator rotations are fixed before the fluence map optimization step.[19]

In our experience, homogeneous radiosurgery plans were more sensitive to isocentre locations than conventional heterogeneous plans where only a rapid dose gradient fall-off is required. A good set of isocentre locations was essential to obtain acceptable homogeneous plans, whereas in heterogeneous radiosurgery plans, the SDO model could account for small variations in isocentre location by modifying the shape of the delivered shot. However, we observed that similar to heterogeneous radiosurgery plans, increasing the number of selected isocentres does not necessarily improve the plan quality.

The average SDO computation time to obtain the inverse plans is 205 min. At the current stage, no particular parallelization of the algorithm is implemented. However, if the algorithm is fully parallelized, a reduction of roughly 80% in computation time is expected. Additionally, better computational power and usage of graphical processing units (GPUs) can improve the computational time by another 50%. The computational time will also improve if more efficient algorithms such as interior point constraint generation[20] are employed for faster and more robust results.

Future work includes designing optimization methods to separate the radiotherapy treatments into individual and potentially unique fractions, as well as more complex scoring techniques based on geometry for isocentre selection.

5. CONCLUSIONS

We have developed an automated inverse planning approach to generate homogeneous dose distributions on PFX to account for OAR-target overlap. The obtained plans achieved improved HI compared to SF-RS plans, while the maximum dose to the brainstem remained within the clinical guideline for all the cases. Our mathematical models for isocentre selection demonstrated that while GTV coverage is relatively easy to obtain, a delicate balance exists between PTV coverage and brainstem dosage when using PFX for homogeneous target dosage. In MF-RS, the large amount of OAR-PTV overlap and the larger target volume (to account for daily setup errors) typically require more isocentres than in SF-RS. The plans obtained in the present study, although not as homogeneous as linac-based plans, demonstrate that PFX has the potential to incorporate treatment margins and overlapping volumes.

ACKNOWLEDGMENTS

The authors would like to thank Håkan Nordström for his assistance with the dose calculation engine and for his comments and suggestions.

This work was funded in part by Elekta Instrument, AB, Stockholm, Sweden, The Canada Foundation for Innovation, The Ontario Research Fund, and the Natural Sciences and Engineering Research Council of Canada (NSERC) PGS-D program.

APPENDIX: ALGORITHMS FOR ISOCENTRE SELECTION

In all the algorithms, the placement option for structure s (p_s) refers to shallow placing, cropping, or regular GSP.

The isocentre selection process begin in Algorithm 1, which requires the user to provide a set of structures $\mathcal{S}$ and placement options for each structure $\mathcal{P}$. In Steps 1–5, artificial regions are added to the set of structures if necessary by calling Algorithm 2 (artificial region creation) for all PTV-OAR overlaps. Note that the original target is removed from the set of structures. Then, the modified GSP algorithm described in Sec. 2.A.5 (mGSP, Algorithm 3) is called for each of the new structures. The isocentres are found in the following order: (1) the overlap volume $\mathcal{OT}$, (2) the expansion ring of the overlap $\text{Ring}_{\mathcal{OT}}$, (3) the central volume $\mathcal{CV}$, and (4) the boundary ring $\mathcal{BR}$. The complete set of selected isocentres, Θ, is returned and used as input into the SDO model.

Note that in Algorithm 3, the score( ) function in Step 17 refers to the original GSP scoring method[7] modified with the

ALGORITHM I. Complete isocentre selection procedure.

Require: $\{\mathcal{S}, \mathcal{P}\} \leftarrow$ ordered set of structures s and placement options p, $r_t \leftarrow$ boundary ring radius of target, $r_o \leftarrow$ expansion radius of OARs
for OARs $\mathcal{O}$ that overlap with PTV $\mathcal{T}$ **do**
  $\{\mathcal{S}', \mathcal{P}'\} \leftarrow$ artificialRegions$(\mathcal{O}, \mathcal{T}, r_t, r_o)$
  $\mathcal{S} \leftarrow \mathcal{S} \cup \mathcal{S}' \setminus \mathcal{T}$
  $\mathcal{P} \leftarrow \mathcal{P} \cup \mathcal{P}'$
end for
$\Theta \leftarrow \emptyset$
for $s \in \mathcal{S}$ **do**
  $\Theta \leftarrow \Theta \cup$ mGSP(s, p_s)
end for
return Θ

ALGORITHM II. Artificial region creation (artificialRegions).

Require: $\mathcal{O} \leftarrow$ organ at risk, $\mathcal{T} \leftarrow$ target, $r_t \leftarrow$ boundary ring radius of pure target $\mathcal{T}'$, $r_o \leftarrow$ expansion radius of $\mathcal{O}$
$\mathcal{OT} \leftarrow \mathcal{O} \cap \mathcal{T}$
$\mathcal{OT}^{exp} \leftarrow \mathcal{OT}$ expanded by radius r_o
$\text{Ring}_{\mathcal{OT}} \leftarrow \mathcal{OT}^{exp} \cap \{\mathcal{T} \setminus \mathcal{OT}\}$
$\mathcal{T}' \leftarrow$ voxels in $\mathcal{T} \setminus \mathcal{OT} \setminus \text{Ring}_{\mathcal{OT}}$
if volume of $\mathcal{T}' \geq 10$ cm^3 **then**
  Perform grassfire algorithm on $\mathcal{T}'$ to obtain depth of every voxel
  $\mathcal{BR} \leftarrow$ voxels in $\mathcal{T}'$ with depth $\leq r_t$
  $\mathcal{CV} \leftarrow$ voxels in $\mathcal{T}' \setminus \mathcal{BR}$
else
  $\mathcal{BR} \leftarrow \emptyset$
  $\mathcal{CV} \leftarrow \emptyset$
end if
return $\mathcal{S} = \{\mathcal{OT}, \text{Ring}_{\mathcal{OT}}, \mathcal{CV}, \mathcal{BR}, \mathcal{T}'\}$, $\mathcal{P} =$ {none, shallow placing, shallow placing, none, none}

ALGORITHM III. Modified grassfire and sphere-packing algorithm (mGSP).

Require: $\{s, p_s\} \leftarrow$ current structure and placement option
$M \leftarrow$ number of isocentres to choose in s
$\Theta \leftarrow \emptyset$
$f \leftarrow 0.15$
for $1, \ldots, M$ **do**
  $d \leftarrow 0$, $s' \leftarrow s$
  while $s' \neq \emptyset$ **do**
    $d \leftarrow d + 1$
    $\mathcal{I}_d \leftarrow$ set of voxels that comprise the outer layer of s' (voxels have depth d)
    $s' \leftarrow s' \setminus \mathcal{I}_d$
  end while
  $r = \arg\max_{r' \in \{4,8,16\}} \{r' : (1 - f)r' \leq 2d\}$
  if $p_s =$ shallow placing option **then**
    $\mathcal{I} \leftarrow \mathcal{I}_r$
  else
    $\mathcal{I} \leftarrow \mathcal{I}_d$
  end if
  $\sigma_i \leftarrow \text{score}(i, r_i), \forall i \in \mathcal{I}$
  $\theta \leftarrow \arg\max_{i \in \mathcal{I}} \{\sigma_i\}$
  $\Theta \leftarrow \Theta \cup \{\theta\}$
  $s \leftarrow s \setminus \text{sphere}(\theta, r_\theta)$ (remove sphere centred at θ with radius r_θ)
end for
return Θ

improved voxel-to-boundary distance calculation described in Sec. 2.A.2. Step 6 in Algorithm 2 calls the original grassfire algorithm[15] to obtain voxel depths.

[a]Electronic mail: kimia@mie.utoronto.ca
[b]Present Address: Innovative Scheduling Inc., Gainesville, Florida 32641.

[1]T. Korytko, T. Radivoyevitch, V. Colussi, B. W. Wessels, K. Pillai, R. J. Maciunas, and D. B. Einstein, "12 Gy gamma knife radiosurgical volume is a predictor for radiation necrosis in non-AVM intracranial tumors," Int. J. Radiat. Oncol., Biol., Phys. **64**, 419–424 (2006).
[2]M. Ruschin, N. Nayebi, P. Carlsson, K. Brown, M. Tamerou, W. Li, N. Laperriere, A. Sahgal, Y.-B. Cho, C. Ménard, and D. Jaffray, "Performance of a novel repositioning head frame for gamma knife perfexion and image-guided linac-based intracranial stereotactic radiotherapy," Int. J. Radiat. Oncol., Biol., Phys. **78**, 306–313 (2010).
[3]M. Ruschin, P. T. Komljenovic, S. Ansell, C. Ménard, G. Bootsma, Y.-B. Cho, C. Chung, and D. Jaffray, "Cone beam computed tomography image guidance system for a dedicated intracranial radiosurgery treatment unit," Int. J. Radiat. Oncol., Biol., Phys. **85**(1), 243–250 (2012).
[4]International Commission on Radiation Units and Measurements, "Prescribing, recording, and reporting photon beam therapy," ICRU Report No. 50 (ICRU Publications, Washington, DC, 1993).
[5]International Commission on Radiation Units and Measurements, "Prescribing, recording, and reporting photon beam therapy," ICRU Report No. 62 (ICRU Publications, Washington, DC, 1999).
[6]International Commission on Radiation Units and Measurements, "Prescribing, recording, and reporting intensity-modulated photon-beam therapy (IMRT)," ICRU Report No. 83 (ICRU Publications, Washington, DC, 2010).
[7]K. Ghobadi, H. R. Ghaffari, D. M. Aleman, D. A. Jaffray, and M. Ruschin, "Automated treatment planning for a dedicated multisource intra-cranial radiosurgery treatment unit using projected gradient and grassfire algorithms," Med. Phys. **39**, 3134–3141 (2012).
[8]Q. J. Wu, S. Jitprapaikulsarn, B. Mathayomchan, D. B. Einstein, R. J. Maciunas, K. Pillai, B. W. Wessel, T. J. Kinsella, and V. Chankong, "Clinical evaluation of a Gamma Knife inverse planning system," Radiosurgery **5**, 260–266 (2004).
[9]Q. J. Wu, V. Chankong, S. Jitprapaikulsarn, B. W. Wessel, D. B. Einstein, T. J. Kinsella, and B. Mathayomchan, "Real-time inverse planning for Gamma Knife radiosurgery," Med. Phys. **30**, 2988–2995 (2003).
[10]M. C. Ferris, J. Lim, and D. M. Shepard, "An optimization approach for radiosurgery treatment planning," SIAM J. Optim. **13**, 921–937 (2002).
[11]M. C. Ferris, J. Lim, and D. M. Shepard, "Radiosurgery treatment planning via nonlinear programming," Ann. Operat. Res. **119**, 247–260 (2003).
[12]M. C. Ferris, J. Lim, and D. M. Sheperd, "Optimization of Gamma Knife radiosurgery," in *Discrete Mathematical Problems with Medical Applications*, DIMACS Series in Discrete Mathematics and Theoretical Computer Science Vol. 55, edited by D.-Z. Du, P. Pardolas, and J. Wang (American Mathematical Society, 2000), pp. 27–44.
[13]T. H. Wagner, T. Yi, S. L. Meeks, F. J. Bova, B. L. Brechner, Y. Chen, J. M. Buatti, W. A. Friedman, K. D. Foote, and L. G. Bouchet, "A geometrically based method for automated radiosurgery planning," Int. J. Radiat. Oncol., Biol., Phys. **48**, 1599–1611 (2000).
[14]B. Wu, F. Ricchetti, G. Sanguineti, T. McNutt, M. Kazhdan, P. Simari, M. Chuang, R. Taylor, and R. Jacques, "Patient geometry-driven information retrieval for IMRT treatment plan quality control," Med. Phys. **36**, 5497–5505 (2009).
[15]H. Blum, "A transformation for extracting new descriptors of shape," in *Models for the Perception of Speech and Visual Form*, edited by W. Wathen-Dunn (MIT Press, Cambridge, 1967), pp. 362–380.
[16]E. Shaw, R. Kline, M. Gillin, L. Souhami, A. Hirschfeld, R. Dinapoli, and L. Martin, "Radiation therapy oncology group: Radiosurgery quality assurance guidelines," Int. J. Radiat. Oncol., Biol., Phys. **27**, 1231–1239 (1993).
[17]D. Schlesinger, Z. Xu, F. Taylor, C. P. Yen, and J. Sheehan, "Interfraction and intrafraction performance of the gamma knife extend system for patient positioning and immobilization: Clinical article," J. Neurosurg. **117**, 217–224 (2012).

[18]E. Tryggestad, M. Christian, E. Ford, C. Kut, Y. Le, G. Sanguineti, D. Song, and L. Kleinberg, "Inter- and intrafraction patient positioning uncertainties for intracranial radiotherapy: A study of four frameless, thermoplastic mask-based immobilization strategies using daily cone-beam CT," Int. J. Radiat. Oncol., Biol., Phys. **80**, 281–290 (2011).

[19]H. Romeijn and J. Dempsey, "Intensity modulated radiation therapy treatment plan optimization," TOP **16**, 215–243 (2008).

[20]M. Oskoorouchi, H. Ghaffari, T. Terlaky, and D. Aleman, "An interior-point constraint generation method for semi-infinite linear programming with health care application," Oper. Res. **59**, 1184–1197 (2011).